

Estimation of interval velocity and attenuation anisotropy from reflection data at the Coronation Field

Jyoti Behura^{†‡}, Ilya Tsvankin[‡], Edward Jenner[§], and Alex Calvert^{§§}, [‡]Center for Wave Phenomena, Colorado School of Mines; [†]currently BP Americas, Houston; [§]ION Geophysical, Denver; ^{§§}currently Maersk Oil, Denmark

SUMMARY

Attenuation can be extremely valuable in characterizing gas sands. In fractured reservoirs, anisotropy can provide additional information about the distribution of fractures. Here, we apply a layer-stripping approach to wide-azimuth P-wave data acquired over a gas reservoir in the Coronation Field, Alberta. The main processing steps involve estimation of traveltimes from the top and bottom of the target layer followed by computation of the interval attenuation using the spectral-ratio method.

The vertical attenuation coefficient shows a reasonable correspondence with existing gas-producing well locations and serves as an indicator of gas accumulation in pore spaces. Based on the attenuation information, we infer that the lower half of the survey area has significant gas reserves. In these areas, the estimated azimuthal anisotropy can be used to plan horizontal wells oriented orthogonal to the fracture direction.

INTRODUCTION

Laboratory studies clearly indicate that attenuation is closely related to fluid saturation and mobility (Spencer, 1979; Gautam *et al.*, 2003). Well-log analysis shows that P-wave attenuation is higher in gas-bearing rocks than in those saturated with oil or water. Extremely low P-wave quality factors (Q), ranging between 5 and 10, have been observed in some gas reservoirs.

Attenuation anisotropy might carry valuable information about fluid- or gas-filled fractures. In fact, preferential flow of fluids in rocks is believed to be the primary cause of attenuation anisotropy (e.g., Mavko & Nur, 1979). Using different fluid-flow models, Pointer *et al.* (2000) show that aligned fluid-filled cracks can result in anisotropic attenuation. Parra *et al.* (2002) observe low Q -values from cross-well studies in fractured zones of a shale-sand sequence. They also find strong attenuation anisotropy with the vertical attenuation coefficient five times larger than the horizontal coefficient.

Behura & Tsvankin (2009a) introduce a layer-stripping technique to extract interval attenuation from reflection data using a variation of the spectral-ratio method (Johnston & Toksöz, 1981). While no information about velocity and attenuation anywhere in the medium is required, the overburden has to be laterally homogeneous with a horizontal symmetry plane. Using synthetic examples for vertical transverse isotropy (VTI) and orthorhombic models, Behura & Tsvankin (2009a) demonstrate that this algorithm can successfully estimate interval anisotropic attenuation in 2D and 3D. Here, we apply this technique to wide-azimuth data acquired at Coronation Field, Alberta and investigate the spatial distribution of gas accumulation and fracturing using the obtained velocity and

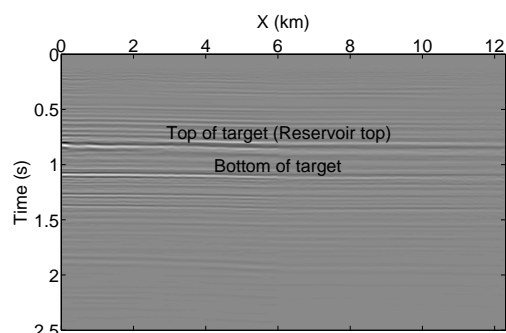


Fig. 1: Seismic section spanning the whole length of the survey. The reflectors bounding the interval of interest are marked.

attenuation fields.

GEOLOGIC SETTING

The Coronation Field is a gas reservoir located in East Central Alberta. The reservoir is part of the Western Canadian Sedimentary Basin with the hydrocarbon production mostly from the Mannville Group. The Mannville Group is of Cretaceous age and corresponds to a major episode of subsidence and sedimentation following a long period of uplift, exposure, and erosion of older strata (Putnam, 1982). The Mannville Group is usually divided into the Upper and Lower Mannville units based on sandstone lithology; the Lower unit is more rich in quartz and chert while the Upper unit has a more feldspathic and volcanic composition. Light oil and gas are usually trapped in numerous fluvial and valley-fill reservoir sandstones, while heavy oil is found in more regionally extensive shoreline sand complexes in the northern and central parts of Alberta and Saskatchewan.

The interval of primary interest at Coronation Field is the Rex member of the Mannville Group (Monk *et al.*, 2006). The sand channels immediately underlie the coals of the Rex member and could vary in thickness from 4 m to 10 m. The width of these channel systems ranges between 200 m and 300 m. Because of the high cost of developing this field, drilling success is critical.

DATA ACQUISITION AND PROCESSING

To understand the lithology of the channel sands and help optimize well placement, Apache Corporation acquired a 3D multicomponent seismic survey (now owned by VGS Seismic Canada Inc.). In this study, we use only the vertical-component data to estimate P-wave velocity and attenuation. The entire survey was shot using single-hole dynamite on a “shoot and roll” template of 12×94

Interval attenuation at Coronation Field

Survey type	3D 3-C
Shot interval (single hole dynamite)	42.43 m
Shot line interval	240 m
Receiver interval	30 m
Receiver line interval	210 m
Receiver patch	12 × 94
Total survey shots	11174
Total survey receivers	11255
Nominal fold (30 m × 30 m bins)	140
Maximum offset	2060 m

Table 1: Acquisition parameters of the survey (Monk *et al.*, 2006).

receivers (Table 1) with the source at the center of the patch. This shooting template is roughly square yielding an excellent azimuthal and offset distribution. The shot lines are oblique to the receiver lines. The subsurface structure is fairly close to layer-cake (no structural dip, Figure 1), which facilitates the layer-stripping technique described in Behura & Tsvankin (2009a).

Prior to attenuation analysis, refraction statics corrections were applied to the data, which were shifted to a smooth floating datum. Some traces were subsequently edited to remove spikes and random noise. Denoising was followed by three passes of residual statics corrections. The ground roll was suppressed using f-k filtering followed by surface-consistent median gain applied to account for the variation in the dynamite source strength.

The most critical step in estimating interval parameters is to pick traveltimes of reflections from the top and bottom of the target layer which can be done using either an auto-picker or semblance analysis. Here, we use the 3D nonhyperbolic semblance algorithm of Vasconcelos & Tsvankin (2006) for orthorhombic media based on the generalized Alkhalifah-Tsvankin Alkhalifah & Tsvankin (1995) equation:

$$t^2(x, \alpha) = t_0^2 + \frac{x^2}{V_{\text{nmo}}^2(\alpha)} - \frac{2\eta(\alpha)x^4}{V_{\text{nmo}}^2(\alpha)[t_0^2 V_{\text{nmo}}^2(\alpha) + (1 + 2\eta(\alpha))x^2]}, \quad (1)$$

where t is the reflected traveltime, x is the offset, t_0 is the two-way zero-offset traveltime, α is the source-to-receiver azimuth, $V_{\text{nmo}}(\alpha)$ is the azimuthally-varying normal-moveout velocity, and $\eta(\alpha)$ is the “anellipticity” coefficient responsible for the deviation from hyperbolic moveout at long offsets. The velocity $V_{\text{nmo}}(\alpha)$ is obtained from the equation of the NMO ellipse:

$$V_{\text{nmo}}^{-2}(\alpha) = \frac{\sin^2(\alpha - \varphi)}{[V_{\text{nmo}}^{(1)}]^2} + \frac{\cos^2(\alpha - \varphi)}{[V_{\text{nmo}}^{(2)}]^2}; \quad (2)$$

φ is the azimuth of the $[x_1, x_3]$ symmetry plane, and $V_{\text{nmo}}^{(1)}$ and $V_{\text{nmo}}^{(2)}$ are the NMO velocities in the vertical symmetry planes $[x_2, x_3]$ and $[x_1, x_3]$, respectively. The parameter η is approximately given by (Pech & Tsvankin, 2004; Xu

& Tsvankin, 2006):

$$\eta(\alpha) = \eta^{(1)} \sin^2(\alpha - \varphi) + \eta^{(2)} \cos^2(\alpha - \varphi) - \eta^{(3)} \sin^2(\alpha - \varphi) \cos^2(\alpha - \varphi), \quad (3)$$

where $\eta^{(1)}$, $\eta^{(2)}$, and $\eta^{(3)}$ are the anellipticity coefficients defined in the $[x_2, x_3]$, $[x_1, x_3]$, and $[x_1, x_2]$ symmetry planes, respectively.

For stratified media, equation 1 has to be applied with effective moveout parameters. Also, equation 3 has to be modified by introducing an additional angle φ_η (Xu & Tsvankin, 2006):

$$\eta(\alpha) = \eta^{(1)} \sin^2(\alpha - \varphi_\eta) + \eta^{(2)} \cos^2(\alpha - \varphi_\eta) - \eta^{(3)} \sin^2(\alpha - \varphi_\eta) \cos^2(\alpha - \varphi_\eta). \quad (4)$$

For aligned vertical symmetry planes in all layers, $\varphi_\eta = \varphi$. The semblance algorithm estimates the parameters of the NMO ellipse ($V_{\text{nmo}}^{(1,2)}$ and φ), the anellipticity parameters $\eta^{(1,2,3)}$ and the azimuth φ_η .

The semblance algorithm of Vasconcelos & Tsvankin (2006) is designed to operate on CMP gathers. Implementation of the layer-stripping algorithm described in Behura & Tsvankin (2009a), however, requires traveltime surfaces on source and receiver gathers. By assuming not just the overburden, but also the target layer to be laterally homogeneous, one can apply semblance analysis based on equation 1 to source and receiver gathers. Since we need the horizontal slowness at both the source and receiver locations, the best-fit effective moveout parameters are computed for the source as well as receiver gathers. The wide-azimuth reflection traveltimes for the top and bottom of the target layer are then used for estimating the interval traveltime, as described by Dewangan & Tsvankin (2006) in 2D and Wang & Tsvankin (2009) for 3D wide-azimuth data.

The interval traveltime and windowed events along the moveout curves serve as the input data to estimate the interval attenuation coefficient using the technique of Behura & Tsvankin (2009a). The presence of notches in the source amplitude spectra complicates the Q -estimation using the spectral-ratio method. To overcome this problem, we compute the instantaneous Q at every frequency followed by median filtering to eliminate spikes. The resulting average over the Q values is taken as a measure of attenuation along the raypath. The additional advantage of computing the instantaneous Q is that it provides a measure of the variance of the normalized phase attenuation coefficient $\mathcal{A} = 1/2Q$.

Assuming velocity anisotropy to have orthorhombic symmetry, we invert for the moveout parameters by fitting equation 1 to the interval traveltimes. The attenuation-anisotropy parameters are estimated by fitting the P-wave phase attenuation function \mathcal{A}_P in orthorhombic media (Zhu & Tsvankin, 2007) to the estimated interval attenuation coefficients:

$$\mathcal{A}_P(\theta, \phi) = \mathcal{A}_{P0} [1 + \delta_Q(\phi) \sin^2 \theta \cos^2 \theta + \epsilon_Q(\phi) \sin^4 \theta], \quad (5)$$

where \mathcal{A}_{P0} is the vertical attenuation coefficient, θ and ϕ are the polar and azimuthal phase angles, respectively,

Interval attenuation at Coronation Field

and

$$\delta_Q(\phi) = \delta_Q^{(1)} \sin^2(\phi - \varphi_Q) + \delta_Q^{(2)} \cos^2(\phi - \varphi_Q), \quad (6)$$

$$\begin{aligned} \epsilon_Q(\phi) = & \epsilon_Q^{(1)} \sin^4(\phi - \varphi_Q) + \epsilon_Q^{(2)} \cos^4(\phi - \varphi_Q) \\ & + (2\epsilon_Q^{(2)} + \epsilon_Q^{(3)}) \sin^2(\phi - \varphi_Q) \cos^2(\phi - \varphi_Q). \end{aligned} \quad (7)$$

The angle φ_Q is the azimuth of the $[x_1, x_3]$ symmetry plane and the parameters $\delta_Q^{(1)}$, $\delta_Q^{(2)}$, $\epsilon_Q^{(1)}$, $\epsilon_Q^{(2)}$, and $\epsilon_Q^{(3)}$ govern the angular variation of the P-wave attenuation coefficient (Zhu & Tsvankin, 2007). We do not assume the same orientation for attenuation as estimated for velocity anisotropy.

Although equation 5 describes the angular variation of the phase attenuation coefficient \mathcal{A} , it is valid for the group attenuation coefficient \mathcal{A}_g estimated from seismic data because $\mathcal{A}_g = \mathcal{A}|_{\xi=0^\circ}$ (Behura & Tsvankin, 2009b). As discussed by Behura & Tsvankin (2009a), inversion for the attenuation-anisotropy parameters requires knowledge of the anisotropic velocity field which can be used to compute the phase angle from the measured group angle. We use a well-log derived interval vertical P-wave velocity V_{P0} of 5000 m/s (Monk *et al.*, 2006) to estimate the velocity anisotropy parameters $\delta^{(1,2,3)}$ and $\epsilon^{(1,2)}$ from the moveout parameters. Using the obtained velocity model, we compute the phase angles from the group angles. Note that it is possible to perform velocity analysis prior to attenuation processing using the interval traveltime because the influence of attenuation on velocity for a fixed frequency typically is of the second order (Zhu & Tsvankin, 2006; Behura & Tsvankin, 2009b).

RESULTS

Here, we discuss the results of azimuthal velocity and attenuation analysis for an interval at about 0.8 s containing the reservoir (Figure 1). The interval NMO ellipse of the target layer is represented by its eccentricity and the azimuth φ^{fast} of the major axis (Figure 2) for each common midpoint. The nmo eccentricity is defined as $|V_{nmo}^{(1)} - V_{nmo}^{(2)}| / V_{nmo}^{fast}$ where $V_{nmo}^{fast} = \max\{|V_{nmo}^{(1)}|, |V_{nmo}^{(2)}|\}$. The lower half of the survey area shows strong azimuthal velocity anisotropy within the target layer, while in the upper half it is weaker. If the field has only one dominant fracture set, the major axis of the NMO ellipse would be parallel to the fractures. This would also imply that in the lower half of the survey area, the target layer is more intensely fractured than it is in the upper half. For increased production, horizontal wells should be drilled orthogonal to the fracture strike. In the presence of more than one fracture set, however, interpretation of NMO ellipses becomes more complicated. Additional data such as well-bore resistivity images could help resolve this ambiguity.

The vertical attenuation coefficient \mathcal{A}_0 is displayed in Figure 3. Zones of higher attenuation (hot colors) in the lower half of the survey area show a reasonable correspondence with locations of existing gas-producing wells (Monk *et al.*, 2006). Therefore, \mathcal{A}_0 could possibly be used as a reliable indicator of gas distribution. In particular, the area in the vicinity of $x = 9$ km, $y = 3$ km possibly

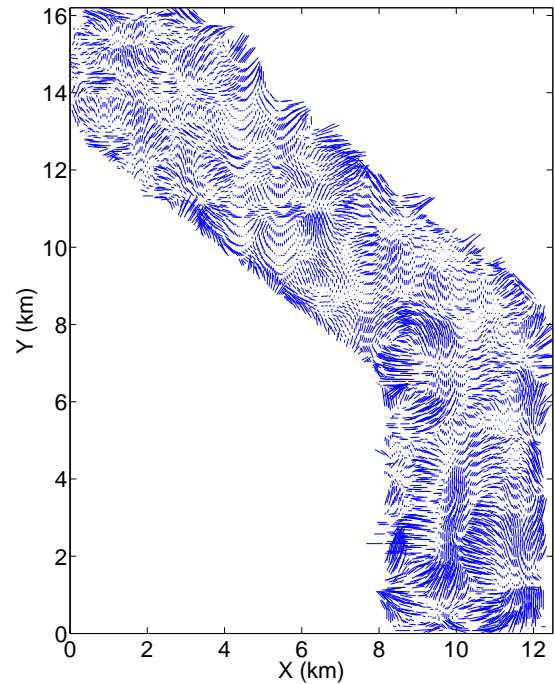


Fig. 2: Eccentricity (tick lengths) and azimuth φ^{fast} (tick orientations) of the interval NMO ellipses in the target layer. The azimuths are computed with respect to the x -axis.

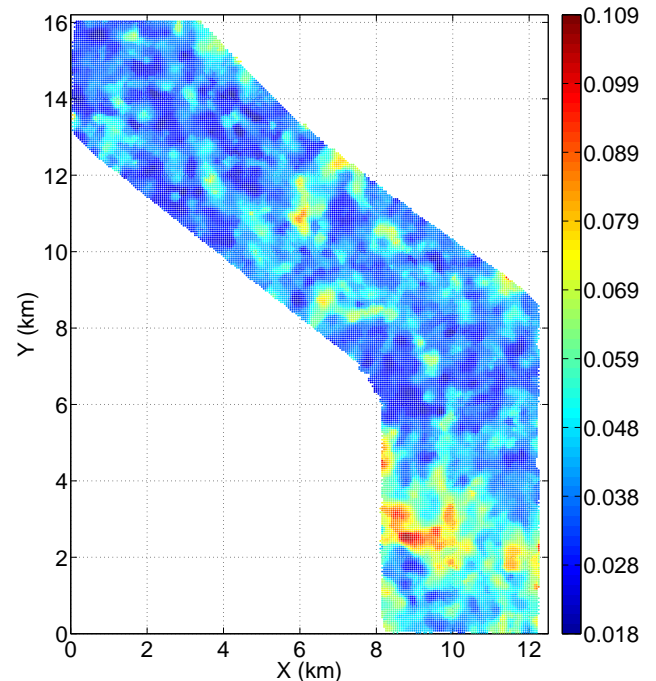


Fig. 3: Interval vertical attenuation coefficient $\mathcal{A}_0 = 1/2Q_0$ for the target layer.

Interval attenuation at Coronation Field

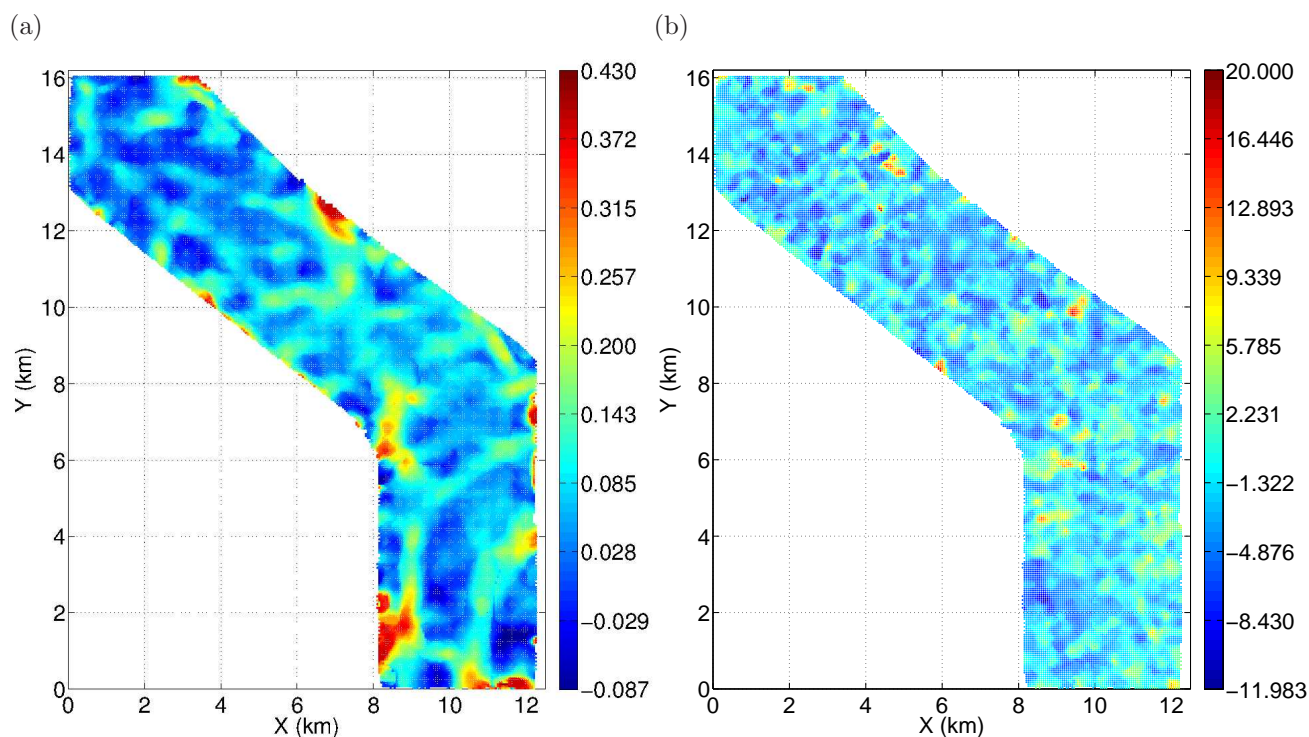


Fig. 4: Velocity-anisotropy parameter δ_1 (a) and attenuation-anisotropy parameter $\delta_Q^{(1)}$ (b).

has large gas accumulations. The coefficient \mathcal{A}_0 should be sensitive to gas present in pores but not to vertical fractures; it should, therefore, be used as an indicator of gas accumulation within the pore space. It is interesting to note that the quality factor of these gas sands can be as low as 5. Note that \mathcal{A}_0 corresponds to the effective attenuation of the whole target layer that includes lithologies other than gas sands.

The magnitude of the attenuation-anisotropy parameters $\delta_Q^{(1)}$ (Figure 4b) and $\delta_Q^{(2)}$ reaches large absolute values approaching 20. Thus, attenuation anisotropy is significantly higher than velocity anisotropy characterized by average δ -values about 0.2 (Figure 4a). Similar observations of stronger anisotropy of attenuation than that of velocity have also been made by Hosten *et al.* (1987), Arts & Rasolofosaon (1992), and Zhu *et al.* (2007). Although the attenuation anisotropy is large, it shows no large-scale spatially coherent patterns within the survey area.

To obtain a measure of azimuthal attenuation anisotropy, we compute the difference $|\delta_Q^{(1)} - \delta_Q^{(2)}|$. Like $\delta_Q^{(1)}$ and $\delta_Q^{(2)}$, this difference varies almost chaotically over the area. The lack of a consistent pattern in the azimuth φ_Q^{max} of the symmetry plane also suggests that attenuation is either azimuthally isotropic or the azimuthal variation is below the noise level.

Well planning should take both interval velocity anisotropy and the attenuation coefficient into account. The optimal strategy would be to drill horizontal wells orthogonal to the fractures in the lower half of the survey area where attenuation anomalies should correspond to

gas accumulations.

CONCLUSIONS

P-wave interval attenuation analysis provides valuable information for reservoir characterization at the Coronation Field. The interval anisotropic velocity and attenuation fields within a subsurface zone containing the reservoir sands were estimated using the layer-stripping approach introduced by Behura & Tsvankin (2009a). Nonhyperbolic semblance analysis yields the wide-azimuth traveltimes for reflections from the top and bottom of the reservoir. Then velocity-independent layer-stripping is employed to generate interval traveltime surfaces. The windowed events along the moveout curves are used for computing the interval anisotropic attenuation.

The lower half of the survey area shows strong azimuthal velocity anisotropy as well as high attenuation. Areas of large interval vertical attenuation coefficient \mathcal{A}_0 correlate with locations of gas-producing wells, which makes \mathcal{A}_0 a reliable indicator of gas sands. At the locations of these anomalously high \mathcal{A}_0 , the orientation of the estimated NMO ellipses can be used to plan horizontal wells. The interval attenuation anisotropy is anomalously strong but does not show a spatially coherent pattern.

ACKNOWLEDGMENTS

We thank ION Geophysical and VGS Seismic for providing the field data and for permission to publish this work.

EDITED REFERENCES

Note: This reference list is a copy-edited version of the reference list submitted by the author. Reference lists for the 2011 SEG Technical Program Expanded Abstracts have been copy edited so that references provided with the online metadata for each paper will achieve a high degree of linking to cited sources that appear on the Web.

REFERENCES

- Alkhalifah, T., and I. Tsvankin, 1995, Velocity analysis for transversely isotropic media: *Geophysics*, **60**, 1550–1566, [doi:10.1190/1.1443888](https://doi.org/10.1190/1.1443888).
- Arts, R. J., and P. N. J. Rasolofosaon, 1992, Approximation of velocity and attenuation in general anisotropic rocks: 62nd Annual International meeting, SEG, Expanded Abstracts, 640–643.
- Behura, J., and I. Tsvankin, 2009a, Estimation of interval anisotropic attenuation from reflection data: *Geophysics*, **74**, no. 6, A69–A74, [doi:10.1190/1.3191733](https://doi.org/10.1190/1.3191733).
- , 2009b, Role of the inhomogeneity angle in anisotropic attenuation analysis: *Geophysics*, **74**, no. 5, WB177–WB191, [doi:10.1190/1.3148439](https://doi.org/10.1190/1.3148439).
- Dewangan, P., and I. Tsvankin, 2006, Velocity-independent layer stripping of PP and PS reflection traveltimes: *Geophysics*, **71**, no. 4, U59–U65, [doi:10.1190/1.2210975](https://doi.org/10.1190/1.2210975).
- Gautam, K., M. L. Batzle, and R. Hofmann, 2003, Effects of fluids on attenuation of elastic waves: 73rd Annual International Meeting, SEG, Expanded Abstracts, 22, 1592–1595.
- Hosten, B., M. Deschamps, and B. R. Tittmann, 1987, Inhomogeneous wave generation and propagation in lossy anisotropic solids — Application to the characterization of viscoelastic composite materials: *Journal of the Acoustical Society of America*, **82**, no. 5, 1763–1770, [doi:10.1121/1.395170](https://doi.org/10.1121/1.395170).
- Johnston, D. H., and M. N. Toksöz, 1981, Seismic wave attenuation: SEG Geophysics Reprint Series No. 2.
- Mavko, G. M., and A. Nur, 1979, Wave attenuation in partially saturated rocks: *Geophysics*, **44**, 161–178, [doi:10.1190/1.1440958](https://doi.org/10.1190/1.1440958).
- Monk, D., R. Larson, and P. Anderson, 2006, An East-Central Alberta multi-component seismic case history. CSEG Recorder, May, 18–22.
- Parra, J. O., C. L. Hackert, and P. Xu, 2002, Characterization of fractured low Q zones at the Buena Vista Hills reservoir, California: *Geophysics*, **67**, 1061–1070, [doi:10.1190/1.1500366](https://doi.org/10.1190/1.1500366).
- Pech, A., and I. Tsvankin, 2004, Quartic moveout coefficient for a dipping azimuthally anisotropic layer: *Geophysics*, **69**, 699–707, [doi:10.1190/1.1759456](https://doi.org/10.1190/1.1759456).
- Pointer, T., E. Liu, and J. A. Hudson, 2000, Seismic wave propagation in cracked porous media: *Geophysical Journal International*, **142**, no. 1, 199–231, [doi:10.1046/j.1365-246x.2000.00157.x](https://doi.org/10.1046/j.1365-246x.2000.00157.x).
- Putnam, P. E., 1982, Fluvial channel sandstones within upper Mannville (Albian) of Lloydminster area, Canada — Geometry, petrography, and paleogeographic implications: *AAPG Bulletin*, **66**, 436–459.
- Spencer, J. W., 1979, Bulk and shear attenuation in Berea Sandstone: The effects of pore fluids: *Journal of Geophysical Research*, **84**, 7521–7523.
- Vasconcelos, I., and I. Tsvankin, 2006, Nonhyperbolic moveout inversion of wide-azimuth P-wave data for orthorhombic media: *Geophysical Prospecting*, **54**, no. 5, 535–552, [doi:10.1111/j.1365-2478.2006.00559.x](https://doi.org/10.1111/j.1365-2478.2006.00559.x).

- Wang, X., and I. Tsvankin, 2009, Estimation of interval anisotropy parameters using velocity-independent layer stripping: *Geophysics*, **74**, no. 5, WB117–WB127, [doi:10.1190/1.3157462](https://doi.org/10.1190/1.3157462).
- Xu, X., and I. Tsvankin, 2006, Anisotropic geometrical-spreading correction for wide-azimuth P-wave reflections: *Geophysics*, **71**, no. 5, D161–D170, [doi:10.1190/1.2335615](https://doi.org/10.1190/1.2335615).
- Zhu, Y., and I. Tsvankin, 2006, Plane-wave propagation in attenuative transversely isotropic media: *Geophysics*, **71**, no. 2, T17–T30, [doi:10.1190/1.2187792](https://doi.org/10.1190/1.2187792).
- , 2007, Plane-wave attenuation anisotropy in orthorhombic media: *Geophysics*, **72**, no. 1, D9–D19, [doi:10.1190/1.2387137](https://doi.org/10.1190/1.2387137).
- Zhu, Y., I. Tsvankin, P. Dewangan, and K. van Wijk, 2007, Physical modeling and analysis of P-wave attenuation anisotropy in transversely isotropic media: *Geophysics*, **72**, no. 1, D1–D7, [doi:10.1190/1.2374797](https://doi.org/10.1190/1.2374797).